

High I_h Channel Density in the Distal Apical Dendrite of Layer V Pyramidal Cells Increases Bidirectional Attenuation of EPSPs

THOMAS BERGER,^{1,*} MATTHEW E. LARKUM,^{2,*} AND HANS-R. LÜSCHER^{1,*}

¹*Institute of Physiology, University of Bern, CH-3012 Bern, Switzerland; and* ²*Abteilung Zellphysiologie, Max-Planck-Institut für Medizinische Forschung, D-69120 Heidelberg, Germany*

Received 19 July 2000; accepted in final form 16 October 2000

Berger, Thomas, Matthew E. Larkum, and Hans-R. Lüscher. High I_h channel density in the distal apical dendrite of layer V pyramidal cells increases bidirectional attenuation of EPSPs. *J Neurophysiol* 85: 855–868, 2001. Despite the wealth of recent research on active signal propagation along the dendrites of layer V neocortical pyramidal neurons, there is still little known regarding the traffic of subthreshold synaptic signals. We present a study using three simultaneous whole cell recordings on the apical dendrites of these cells in acute rat brain slices to examine the spread and attenuation of spontaneous excitatory postsynaptic potentials (sEPSPs). Equal current injections at each of a pair of sites separated by $\sim 500 \mu\text{m}$ on the apical dendrite resulted in equal voltage transients at the other site (“reciprocity”), thus disclosing linear behavior of the neuron. The mean apparent “length constants” of the apical dendrite were 273 and 446 μm for somatopetal and somatofugal sEPSPs, respectively. Trains of artificial EPSPs did not show temporal summation. Blockade of the hyperpolarization-activated cation current (I_h) resulted in less attenuation by 17% for somatopetal and by 47% for somatofugal sEPSPs. A pronounced location-dependent temporal summation of EPSP trains was seen. The subcellular distribution and biophysical properties of I_h were studied in cell-attached patches. Within less than $\sim 400 \mu\text{m}$ of the soma, a low density of $\sim 3 \text{ pA}/\mu\text{m}^2$ was found, which increased to $\sim 40 \text{ pA}/\mu\text{m}^2$ in the apical distal dendrite. I_h showed activation and deactivation kinetics with time constants faster than 40 ms and half-maximal activation at -95 mV . These findings suggest that integration of synaptic input to the apical tuft and the basal dendrites occurs spatially independently. This is due to a high I_h channel density in the apical tuft that increases the electrotonic distance between these two compartments in comparison to a passive dendrite.

INTRODUCTION

Neurons in the CNS integrate thousands of synaptic inputs along their dendrites and generate action potentials representing their output as a function of time, quantity, and frequency. Layer V pyramidal neurons of the neocortex have been used extensively to study these mechanisms. This is mainly due to their long thick apical dendrite, which is readily accessible for electrophysiological studies. The apical dendrite traverses all cortical layers ending in a tuft in layer I. Input on this tuft must spread along a cable-like structure for $\leq 1 \text{ mm}$ before reaching the low-threshold sodium spike initiation zone at the axon initial segment. Without active “boosting,” the synaptic poten-

tial would reach this spike initiation zone greatly attenuated and would thus be nearly ineffective in shaping the output of the neuron. In addition to the sodium spike initiation zone, layer V pyramidal neurons have a second, high-threshold calcium spike initiation zone in the upper half of the apical dendrite (Schiller et al. 1997). This led to the suggestion that distal inputs are functionally separated from proximal ones (Yuste et al. 1994). It is therefore important to understand how both integration sites are functionally coupled by suprathreshold as well as subthreshold signals. The sodium spike is not only the output signal but also propagates back into the apical dendrite (Stuart and Sakmann 1994). There it combines with distal input and the two initiation sites interact in a highly nonlinear fashion (Larkum et al. 1999a,b).

Various dendritic conductances may influence subthreshold events in neocortical pyramidal neurons (for review, see Johnston et al. 1996; Magee 1999b; Yuste and Tank 1996). The most profound effects on small membrane deflections seem to be due to the hyperpolarization-activated cation current I_h (Schwindt and Crill 1997; Stuart and Spruston 1998), which is active at resting membrane potential (Pape 1996). I_h significantly alters the attenuation and summation of dendritic events in pyramidal neurons (Magee 1999a; Williams and Stuart 2000).

In this study, we were asking the following questions. How much are spontaneous excitatory postsynaptic potentials (sEPSPs) attenuated along the apical dendrite in both the somatofugal and somatopetal direction? Is this influenced by I_h deactivation? Where is this conductance situated and what are its properties? Spontaneous synaptic events were recorded simultaneously using three patch pipettes along the apical dendrite of layer V pyramidal neurons. Attenuation of sEPSPs in both directions under control conditions and in the presence of an I_h blocker was investigated. Thereafter cell-attached recordings revealed a high I_h density in the distal apical dendrite. The main findings are that not only are EPSPs not “boosted” along the apical dendrite but in fact are more attenuated than expected from a passive uniform cable model due to the inhomogeneous distribution of I_h . This high I_h density introduces a large electric load in the distal apical dendrite, resulting in an increase of the electrotonic distance between the two spike initiation zones and thus confining the integration of

* T. Berger, M. E. Larkum, and H.-R. Lüscher contributed equally to this work.

Address for reprint requests: T. Berger, Institute of Physiology, University of Bern, Bülhlplatz 5, CH-3012 Bern, Switzerland (E-mail: berger@pyl.unibe.ch).

The costs of publication of this article were defrayed in part by the payment of page charges. The article must therefore be hereby marked “advertisement” in accordance with 18 U.S.C. Section 1734 solely to indicate this fact.

synaptic inputs to one or the other spike initiation zone while only the crossing of threshold is effectively transmitted to the other initiation zone.

METHODS

Brain slice preparation and cell identification

Three-hundred-micrometer-thick parasagittal slices of the somatosensory neocortex were prepared from 28- to 34-day-old Wistar rats according to federal and institutional guidelines. This was done in ice-cold extracellular solution using a vibratome (Pelco Series 1000, Redding, CA). Slices were incubated at 37°C for 30–60 min and left at room temperature until recording. Layer V pyramidal neurons from the somatosensory area with a long, thick apical dendrite were visualized by infrared differential interference contrast (IR-DIC) video-microscopy (Stuart et al. 1993) using a Newvicon camera (C2400, Hamamatsu, Hamamatsu City, Japan) and an infrared filter (RG9, Schott, Mainz, Germany) mounted on an upright microscope (Axioskop FS, Zeiss, Oberkochen, Germany). The best recordings with respect to cell quality and ease of access were obtained from dendrites that were barely visible.

Current-clamp recordings

Current-clamp whole cell recordings were made from three sites on the apical dendrite (or alternatively, from 2 sites on the dendrite and 1 on the soma). The compensation of the series resistance across an electrode can sometimes be unreliable for recording fast events—especially when recording while simultaneously passing current. Under these circumstances, it is impossible to know exactly what amount of resistance compensation to use to determine the true membrane potential. This problem is avoided entirely by the use of three electrodes. Thus we are able to measure the true voltage responses at two electrodes while injecting current with a third electrode. We recorded from similar positions across all neurons investigated ($n = 13$) to make general conclusions. Thus we used two $\sim 200\text{-}\mu\text{m}$ segments starting near the soma; this ensured that the main bifurcation of the apical dendrite came after the most distal electrode. The most proximal electrode was located at the soma in five cells and within $100\ \mu\text{m}$ in the remaining eight. The mean interelectrode distances were 233 ± 32 and 202 ± 37 (SD) μm for the proximal and distal dendritic segment, respectively. This gave a mean total distance of $435 \pm 60\ \mu\text{m}$. Three Axoclamp-2B amplifiers (Axon Instruments, Foster City, CA) were used. Bridge balance and capacitance compensation was performed on all three electrodes (borosilicate glass tubing with or without 20% PbO; Hilgenberg, Malsfeld, Germany). The resistance was 5–10 M Ω for somatic and 10–25 M Ω for dendritic recording pipettes. Hyperpolarizing rectangular current pulses were injected consecutively through the three electrodes, and the resulting voltage deflections were simultaneously recorded from all three electrodes. All traces shown are the average of 20 sweeps. For the study of sEPSPs, 1 μM bicuculline methiodide was added to the perfusion solution to block spontaneous inhibitory postsynaptic potentials. Because the occurrence of sEPSPs is a rare and irregular event in the slice preparation, recording periods as long as 30 min were needed to gather a sufficient number of sEPSPs. After a first recording session, 50 μM 4-(*N*-ethyl-*N*-phenylamino)-1,2-dimethyl-6-(methylamino)pyridinium chloride (ZD7288) (Harris and Constanti 1995) or 5 mM CsCl was added to the bath solution to block the hyperpolarization-activated cation current I_h . The current injection experiments were then repeated and sEPSPs again were recorded. Continuous recordings were filtered at 3 kHz and digitized off-line at 10 kHz with 12-bit resolution using a ITC16 A/D converter. Spontaneous EPSPs were stored on a DAT recorder (DTR-1802, Biologic, France). All experiments were done at $\sim 34^\circ\text{C}$.

Voltage-clamp recordings

To study I_h currents, somatic and dendritic whole cell as well as nucleated-patch voltage-clamp recordings (pipette resistance = 2–4 M Ω) were made by means of an Axopatch-200A amplifier (Axon Instruments). To obtain nucleated patches (Sather et al. 1992), negative pressure (100–200 mbar) was applied during the withdrawal of the patch pipette. In cell-attached recordings (pipette resistance = 2.3–5 M Ω), the resting membrane potential (V_m ; -65.3 ± 4.9 mV) was measured at the end after rupture of the cell membrane in the whole cell mode, and recordings with a V_m more positive than -60 mV were discarded. An outside-out patch was excised after each recording; this was essential for multiple cell-attached recordings on the dendrite of the same cell. Data were filtered at 1 kHz using the internal 4-pole low-pass Bessel filter of the amplifier. The sampling frequency was twice the filter frequency. Data were digitized and stored on-line using Clampex8 (Axon Instruments) connected to a personal computer. Data were analyzed off-line with Clampfit8. All cell-attached traces shown represent averages of 5–50 sweeps, while the whole cell data were not averaged. Leak and capacitance of the cell-attached currents were subtracted.

Data analysis of the current-clamp data

The steady-state attenuation of the induced voltage responses were measured during the last 20 ms of the transients produced by long (400 ms, -200 pA) current pulses. The transients recorded with the current injection electrodes were not used for the analysis due to possible series resistance compensation problems.

The following transfer coefficients for the electrode positions i and j were determined (Carnevale and Johnston 1982): transfer resistance, $R_{ij} = V_j/I_i$; coupling coefficient, $k_{ij} = V_j/V_i$; attenuation, $A_{ij} = 1/k_{ij}$.

Linearity was assessed applying the reciprocity test; $R_{ij} = R_{ji}$ (Koch 1999) (see Figs. 1, *A* and *B*, and 5*A*). We took advantage of the use of three electrodes to precisely calculate the input resistance at the middle electrode using the property of transitivity following directly from the definitions given above: $R_{ll} = R_{ij}R_{ij}/R_{ij}$ where l corresponds to the location between location i and j , and R_{ll} corresponds to the input resistance at location l . In this way, determination of input resistance did not depend on series resistance compensation.

Single sEPSPs were fitted with an a-b function (Larkum et al. 1996). Because the decaying phase of sEPSPs always fell below baseline (see Fig. 2), the entire shape of the sEPSP could not be fitted satisfactorily. We therefore restricted the fits to the rising phase of the sEPSPs. In this paper, we analyze the peak amplitude because it was the most reliable parameter. sEPSPs were rarely superimposed because they occurred at a low frequency. Clearly superimposed sEPSPs were not considered.

I_h currents in cell-attached patches

The amplitudes of the hyperpolarization-activated current were normalized to a pipette tip surface of $1\ \mu\text{m}^2$. For the evaluation of the kinetic properties of I_h , we used primarily large-amplitude current recordings from the distal dendrites. The time constants of the kinetics were determined by least-squares fit of the rising or the decaying phase, respectively. Activation and deactivation time courses were evaluated using a fitting interval of 100 ms after the onset and end of the current, respectively (Fig. 9). The amplitudes of the tail currents induced after switching back to V_m from different clamp potentials were plotted and fitted with a Boltzmann function to obtain the activation range of the current (Fig. 10). The reversal potential (E_h) was extrapolated from a linearly fitted I - V curve obtained from the amplitude of the currents after jumping to different holding potentials from a fully activated state. Using the Goldman-Hodgkin-Katz equation the K^+/Na^+ ratio was calculated from E_h .

Pooled data are expressed as means \pm SD, and tests for statistical

differences used an unpaired *t*-test (assuming nonequal variance) with a significance level of 0.05 (*) or 0.01 (**).

Chemicals and solutions

Slices were continuously superfused with a physiological extracellular solution containing (in mM) 125 NaCl, 25 NaHCO₃, 2.5 KCl, 1.25 NaH₂PO₄, 2 CaCl₂, 1 MgCl₂, and 20 glucose, bubbled with 95% O₂-5% CO₂. Pipette solution for current-clamp recordings contained (in mM) 105 K-gluconate, 30 KCl, 10 HEPES, 4 MgCl₂, 2 Na₂ATP, and 0.3 Na₂-GTP, pH adjusted to 7.3 with KOH. Pipette solution for voltage-clamp whole cell recordings contained (in mM) 110 K-gluconate, 30 KCl, 10 EGTA, 10 HEPES, 4 Mg-ATP, 0.3 Na₂-GTP, and 10 Na₂-phosphocreatine, pH adjusted to 7.3 with KOH. Biocytin (0.1–0.5%, wt/vol) was added to the pipette solution to visualize the morphology of the pyramidal neurons. Pipette solution for nucleated patch recordings contained (in mM) 140 KCl, 10 EGTA, 10 HEPES, 4 Mg-ATP, 0.3 Na₂-GTP, and 10 Na₂-phosphocreatine, pH adjusted to 7.3 with KOH. Pipette solution for cell-attached recordings contained (in mM) 120 KCl, 20 TEA-Cl, 5 4-aminopyridine, 10 EGTA, 10 HEPES, 4 Mg-ATP, 0.3 Na₂-GTP, and 10 Na₂-phosphocreatine, pH adjusted to 7.3 with KOH. To study the reversal potential of the I_h current in the cell-attached configuration, we used a high-Na⁺ solution containing (in mM) 110 NaCl, 2.5 KCl, 20 TEA-Cl, 5 4-aminopyridine, 10 EGTA, 10 HEPES, 4 Mg-ATP, 0.3 Na₂-GTP, and 10 Na₂-phosphocreatine, pH adjusted to 7.3 with NaOH.

ZD7288 was a generous gift of Astra-Zeneca (Macclesfield, UK). Tetrodotoxin (TTX) was bought from Alomone Labs (Jerusalem, Israel) and *N*-(2,6-dimethylphenylcarbamoylmethyl)triethylammonium bromide (QX 314) was bought from Tocris Cookson (Bristol, UK). All other drugs and chemicals were from Sigma or Merck. Stock solutions of 300 μM TTX and 50 mM ZD7288 were prepared in bidistilled water. Dilution in the extracellular or in the pipette solution provided the final concentrations given below. QX 314 was added to the pipette solution immediately before use.

Neuron staining and reconstruction

After filling the cell with biocytin, the pipettes were carefully withdrawn and repositioned close to the original location, and a low-power (×5) bright-field image was taken with the video camera. The position of the electrodes was clearly seen on these images, and the distances between the electrodes could be measured to within ~5 μm using a micrometer scale. Finally slices were fixed in 5% paraformaldehyde and subsequently processed using an avidin-horseradish peroxidase reaction (Vector Laboratories, Burlingame, CA) (Hsu et al. 1981) to visualize the cell. Slices were not dehydrated to minimize shrinkage. After coverslipping in Moviol, the stained cells were photographed and reconstructed using computer-assisted reconstruction systems (NeuroLucida or NTS). Only the most proximal part of the axon was reconstructed. For 11 of 13 cells studied in the triple current-clamp experiments the morphology could be obtained.

RESULTS

The results will be presented in the following sequence. First, the membrane potentials at the three recording sites will be summarized. Second, reciprocity test, voltage attenuation, coupling coefficient, and transfer resistance for long hyperpolarizing current pulses will be presented. Third, we will present the coupling coefficients and attenuation properties obtained from sEPSPs. Fourth, we will describe summation properties of the apical dendrite. In all these paragraphs, we will compare the results under control and with block of the hyperpolarization-activated current (I_h). A fifth section summarizes the pharmacological properties of the I_h conductance while in the two

closing sections its subcellular localization and its kinetic properties are described.

Membrane potential

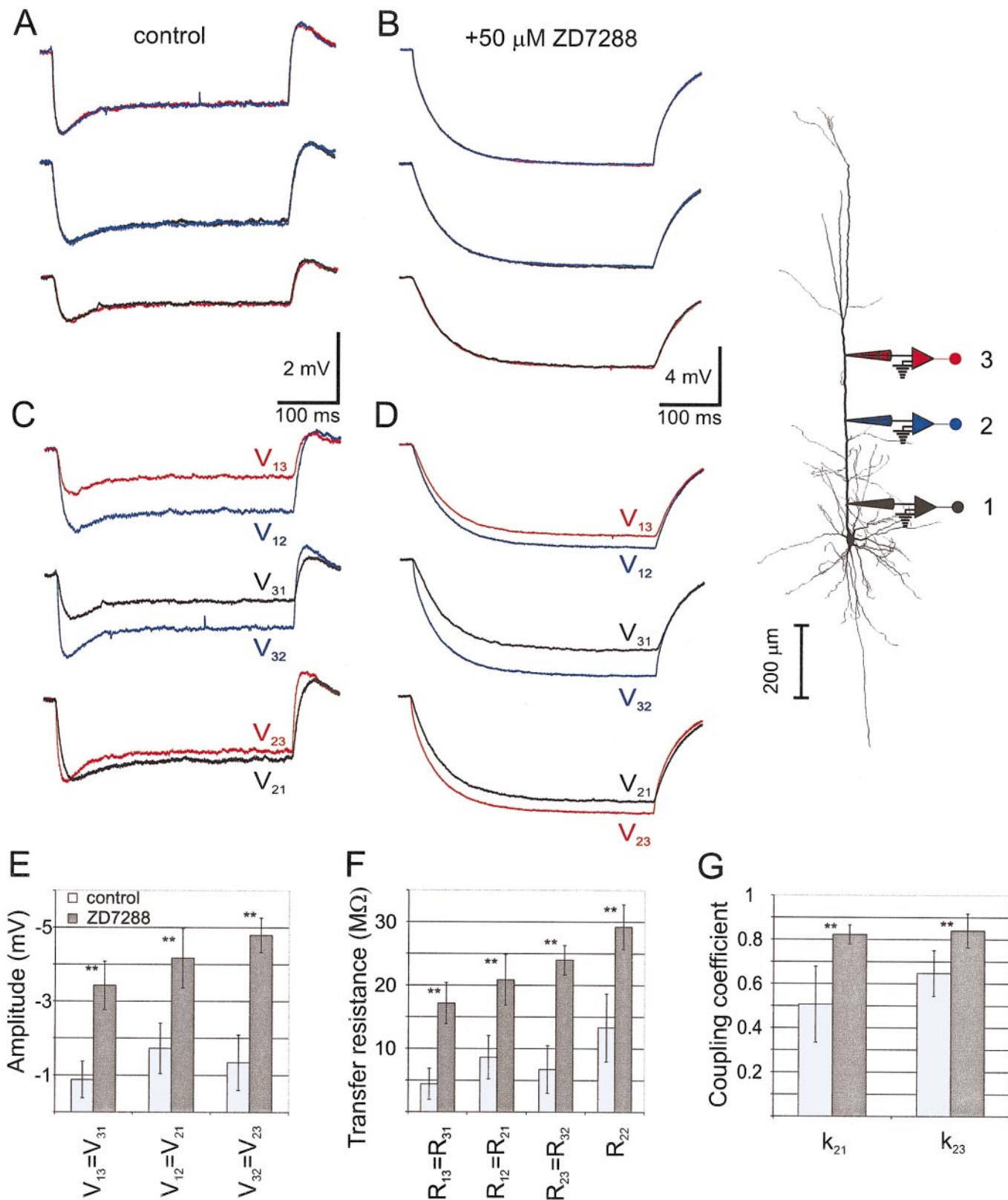
The recorded membrane potential immediately after breakthrough was less negative at the middle and even less negative at the distal electrode than at the proximal electrode: proximal -66.6 ± 7.1 mV, middle -63.0 ± 5.6 mV, distal -60.7 ± 5.0 mV ($n = 13$). After the application of 50 μM ZD7288, a blocker of the I_h current (Harris and Constanti 1995), the membrane potential hyperpolarized significantly more at the distal and middle electrode than at the proximal electrode (proximal -11.0 ± 1.1 mV, middle -13.6 ± 0.5 mV, distal -17.2 ± 0.7 mV; $n = 6$; $P < 0.01$). Thus block of I_h resulted in a similar V_m at the three recording sites.

Reciprocity, voltage attenuation, transfer resistance, and coupling coefficient for hyperpolarizing current pulses

A fundamental property of a linear system is reciprocity. If current is injected at location *i* (e.g., somewhere in the dendritic tree) and the resulting voltage is measured at location *j* (e.g., at the cell body), we record the same voltage at location *i* if the identical current is injected at location *j*. This is a sensitive test for linearity and was used throughout this study. This reciprocity test is illustrated for long, hyperpolarizing (400 ms, -200 pA) current pulses. Pairs of reciprocal recordings are superimposed under control conditions (Fig. 1A; $n = 13$) and after the application of ZD7288 ($n = 6$) or CsCl ($n = 1$; Fig. 1B). The color codes of the voltage traces correspond to the color codes of the electrodes shown in the inset (the same color code is used in all illustrations). Under control conditions, the voltage transients show a prominent sag, indicative of I_h . This sag disappeared completely under ZD7288, confirming the presence of an I_h . The nearly perfect superposition of records from different electrodes suggests that the investigated cells behave linearly for the small voltage range tested around the resting membrane potential, regardless of whether I_h channels are blocked or not. Note, however, that such linear behavior does not imply a homogeneous conductance distribution.

Estimating voltage attenuation from the site of current injection to the recording site is usually difficult because of uncertainties with the series resistance compensation of the electrodes. However, with three simultaneous recording electrodes we did not need to rely on the voltage transients recorded with the current injecting electrode for determining voltage attenuation, transfer resistance, and coupling coefficients. However, the number of coupling coefficients that can be determined is limited to two, namely to k_{21} (coupling coefficient from the middle to the proximal electrode with current injected into the distal electrode), and k_{23} (opposite direction).

Three pairs of voltage transients are shown under control conditions (Fig. 1C) as well as with ZD7288 (Fig. 1D). Current was injected into one electrode while the simultaneously recorded voltage transients from the two other electrodes are displayed. Such recordings were obtained from all 13 cells under control conditions and in seven experiments with I_h block. The pooled data are illustrated in Fig. 1, E–G. As predicted from the reciprocity test, steady-state voltage transfer



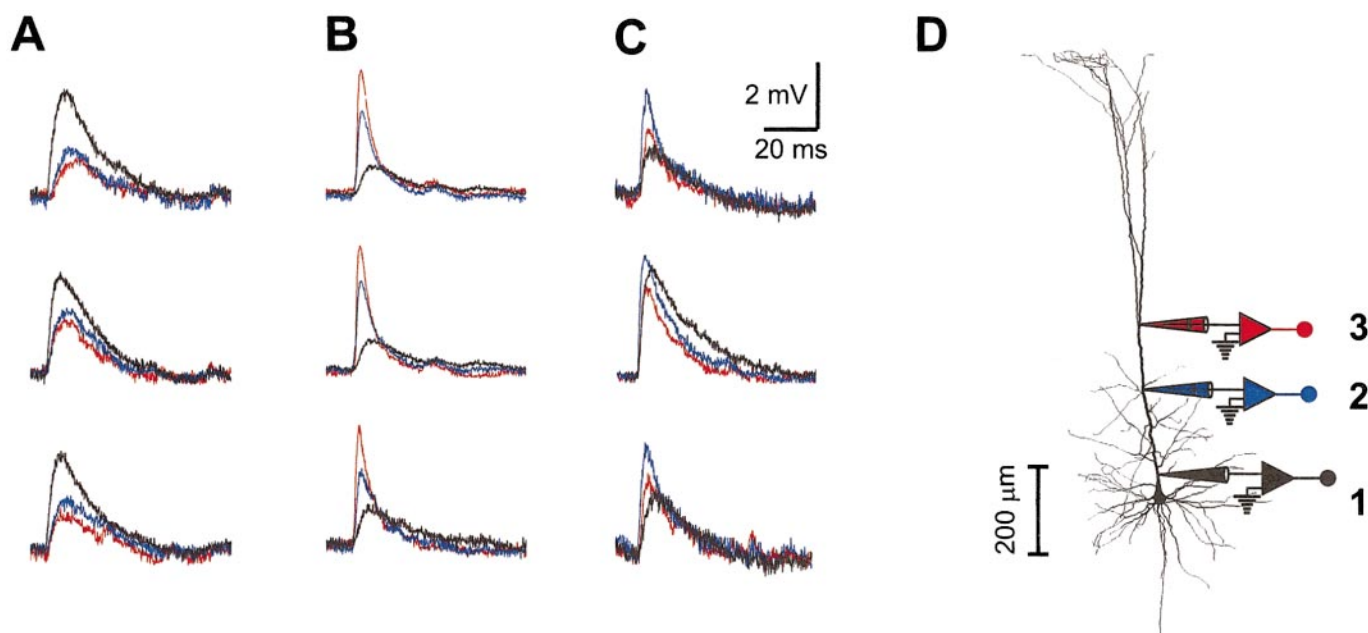


FIG. 2. Simultaneous triple recordings of spontaneous synaptic events from the apical dendrite. A–C: simultaneously recorded spontaneous excitatory postsynaptic potentials (sEPSPs) are superimposed, and the color code corresponds to that of the electrodes shown in D. The presumed site of origin can be judged from the amplitude attenuation, the increase in time to peak, and the increase in latency. There are examples of sEPSPs, which presumably originate at the basal dendrites or soma (A), and recordings, which presumably originate distal to electrode 3 in the tuft (B). Note in this case the crossing of the decaying phases in the 3 sEPSPs. C: examples of 3 sEPSPs that most likely originate close to *electrode 2*, possibly in the oblique dendrites. D: reconstructed P34 pyramidal neuron from which the recordings were obtained, showing the location of the electrodes.

was symmetric ($V_{13} = V_{31}$, -0.8 ± 0.5 mV; i.e., current injected at *electrode 1* and voltage measured at *electrode 3*, and vice versa are identical; true also for $V_{12} = V_{21}$, -1.7 ± 0.7 mV and $V_{23} = V_{32}$, -1.3 ± 0.7 mV; Fig. 1E). Reciprocity was true under control as well as under I_h blocking conditions ($V_{13} = V_{31}$, -3.4 ± 0.6 mV, $V_{12} = V_{21}$, -4.2 ± 0.8 mV, and $V_{23} = V_{32}$, -4.8 ± 0.5 mV; Fig. 1E). The same symmetry was seen for the transfer resistances (Fig. 1F). As expected, mean transfer resistance is lowest from *electrodes 1* to *3* ($R_{13} = R_{31}$; 4.4 ± 2.5 M Ω) due to the long mean distance between the two electrodes. The mean transfer resistance between *electrodes 1* and *2* was 8.6 ± 3.4 M Ω ($R_{12} = R_{21}$) and between *electrodes 2* and *3* 6.7 ± 3.8 M Ω ($R_{23} = R_{32}$). Under I_h blocking conditions, the values increased to 17.1 ± 3.2 , 20.9 ± 4.0 , and 24.0 ± 2.3 M Ω , respectively. Transfer resistances were used to calculate the input resistance of the cells at the middle electrode (formula see METHODS; $R_{22} = 13.3 \pm 5.4$ M Ω under control and 29.2 ± 3.5 M Ω under I_h blocking conditions).

Mean coupling coefficient k_{21} was 0.51 ± 0.17 and k_{23} was 0.65 ± 0.10 under control and 0.82 ± 0.04 and 0.84 ± 0.08 in ZD7288 or CsCl (Fig. 1G). Thus steady-state voltage amplitude, transfer resistance, and coupling coefficient increased significantly after blocking I_h (Fig. 1, E–G).

Coupling coefficients of sEPSPs

Comparing the sEPSPs recorded simultaneously from the three electrodes makes it possible to locate the approximate region of origin for any given synaptic signal (Fig. 2) (see also Larkum et al. 1998 for the issue of separating spontaneous events into populations representing synaptic inputs onto different segments). Identification of the origin of the sEPSPs was established on the following criteria, which are based on a priori knowledge of cable properties (Rall 1967): for sEPSPs originating proximal to the proximal electrode (e.g., soma and/or basal dendrites), the amplitude attenuates, while time to

FIG. 1. Steady-state attenuation, transfer resistance, and coupling coefficient of a layer V pyramidal cell. The dendrite of a layer V pyramidal cell (P30) was patched simultaneously in whole cell mode at 3 sites, and voltage transients were induced under current clamp. A and B: reciprocity test under control conditions (A) and with $50 \mu\text{M}$ 4-(N-ethyl-N-phenylamino)-1,2-dimethyl-6-(methylamino) pyridinium chloride (ZD7288, B). A hyperpolarizing (-200 pA) current pulse was injected alternatively at each of a pair of electrodes, and the resulting voltage response at the other electrode is displayed. For better comparison, these reciprocally obtained traces are superimposed. The color of the traces corresponds to the color code of the recording electrodes. Note the prominent “sag” under control conditions indicating a hyperpolarization-activated current (I_h). Each reciprocal pair superimposes perfectly, suggesting that the investigated neuron behaved as a linear system under these conditions. When the I_h was blocked with ZD7288 (B), the ideal superposition of voltage deflections again indicates linear properties. C and D: steady-state attenuation, transfer resistance, and coupling coefficient studied with the same current injection under control conditions (C) and with ZD7288 (D). Current was injected into one electrode, while the simultaneously recorded voltage transients from the 2 other electrodes are displayed. As in A and B, the color of the traces corresponds to the color code of the recording electrodes. E–G: summary of steady-state voltage amplitude (E), transfer resistance (F), and coupling coefficient (G) under control conditions (light gray bars, $n = 13$) and with ZD7288 (dark gray, $n = 6$). Only 2 coupling coefficients were calculated (k_{21} and k_{23} , but not k_{13}) so that there could be no possible error introduced by series resistance problems. In all experiments, there was always perfect symmetry in voltage attenuation (E) and transfer resistances (F), indicative of a linear system.

peak (tp) and latency of the sEPSPs increase from *electrodes 1 to 2 to 3* (Fig. 2A). The reverse order is seen when the sEPSPs originate distal to *electrode 3* (e.g., in the tuft; Fig. 2B). sEPSPs that were largest at the middle electrode must have originated somewhere between *electrodes 1 and 3* (possibly on an oblique dendrite; Fig. 2C). Distally elicited sEPSPs are on average significantly larger and faster than sEPSPs elicited at the soma or basal dendrites ($V_{\text{proximal}} = 1.6 \pm 0.8$ mV, $V_{\text{distal}} = 2.3 \pm 1.6$ mV; $\text{ttp}_{\text{proximal}} = 4.5 \pm 1.9$ ms, $\text{ttp}_{\text{distal}} = 2.1 \pm 0.9$ ms; $n = 281$ for proximal sEPSPs and $n = 351$ for distal sEPSPs). We chose only events that had the largest amplitude at one of the two outer electrodes. Synaptic contacts given off by a single afferent fiber are not necessarily restricted to a confined region of the neuron. sEPSPs from widely distributed locations should lead to unusual latency progression at the three recording locations and more or less pronounced inflections. Such composite sEPSPs were excluded from the analysis.

Once the origin of the sEPSPs was determined, the coupling coefficients could be estimated by relating their amplitudes recorded from different electrodes. Six coupling coefficients could be determined, namely k_{13} , k_{31} , k_{12} , k_{21} , k_{23} , and k_{32} . The peak amplitudes of sEPSPs measured at the distal electrode were plotted versus the amplitudes measured at the proximal electrode for sEPSPs spreading in somatofugal and somatopetal direction (Fig. 3A). Linear regression lines were fitted through the two data sets. The slope of the regression lines corresponds to the mean coupling coefficient (k_{31}) for somatopetal sEPSPs, while the reciprocal value of the slope of the regression line corresponds to the coupling coefficient (k_{13}) for somatofugal sEPSPs. The coupling coefficient from distal to proximal was, as expected, always smaller than in the opposite direction. Thus sEPSPs transmitted from the soma to the tuft attenuate less than sEPSPs transmitted from the tuft to the soma. Since the sEPSPs are recorded simultaneously with three electrodes, separate coupling coefficients can be determined for the proximal and distal segment. These coupling coefficients are similar for sEPSPs spreading in the same direction (Fig. 3B), and they are approximately twice as large as those determined for sEPSP spreading over the full distance (k_{31} , k_{13}).

In an infinite cable, the logarithm of the signal attenuation is equal to the electrotonic distance between the two points of observation (Zador et al. 1995). This means that the logarithms (ln) of attenuation for different sections of such a cable are additive. We have used this relationship as an approximation to extract the length of the apical dendritic segment over which a typical sEPSP attenuates to $1/e$ in both the somatofugal and the somatopetal direction. In Fig. 3C, ln of mean attenuation is plotted versus dendritic distance for 10 experiments. Six independent attenuation factors could be determined per experiment; three for each direction. Linear regression lines are fitted through the origin and the two data sets. The intersections with ln (mean attenuation) = 1 gives the average physical distance in micrometers over which a sEPSP with an average time course attenuates to $1/e$ spreading from dendrite to soma (273 μm) and from soma to dendrite (446 μm). Thus attenuation is more pronounced for an EPSP spreading from the tuft toward the soma than in the opposite direction. We would like to define these numbers as the AC correlate of the DC length constant. Because EPSPs have different time courses, this definition is an approximation and reflects a mean AC length

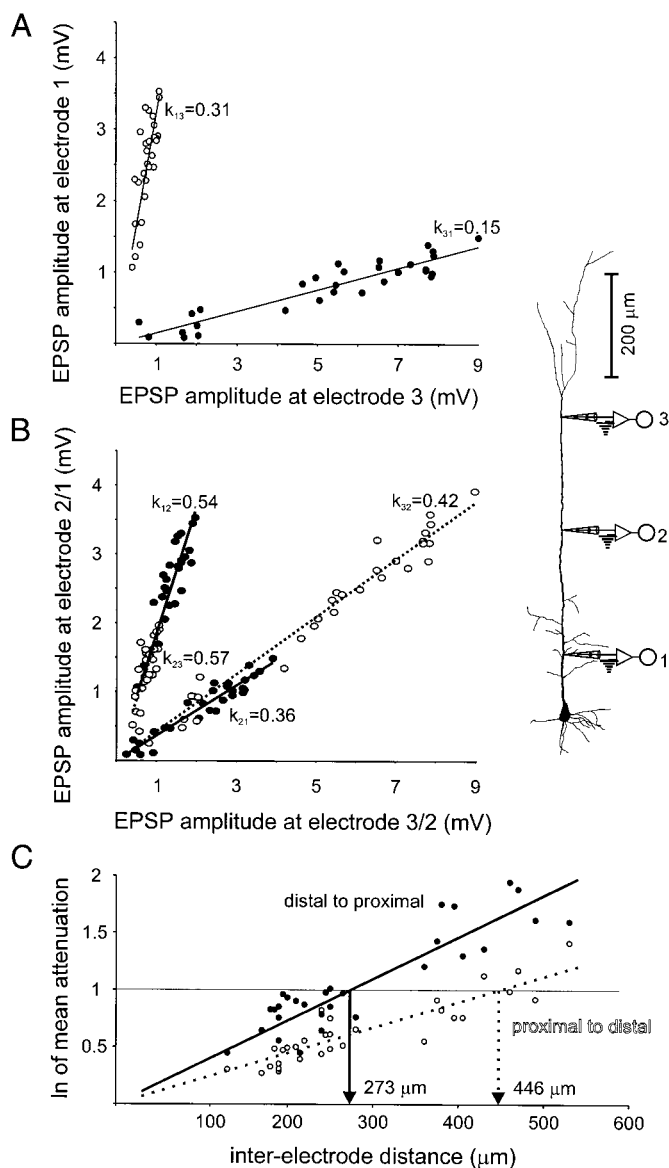


FIG. 3. Determination of coupling coefficients and "AC length constants" for spontaneous EPSPs. *A*: the peak amplitudes of spontaneous sEPSPs measured at the distal *electrode 3* are plotted against the peak amplitudes of the same sEPSPs measured at the proximal *electrode 1*. Filled symbols are from sEPSPs spreading from distal to proximal and open symbols from sEPSPs spreading from proximal to distal. Linear regression lines are fitted through each set of data. Coupling coefficient k_{31} equals the slope of the regression line through the filled symbols, while coupling coefficient k_{13} equals $1/\text{slope}$ of the regression line through the open symbols. *B*: coupling coefficients determined as in *A* but for the dendritic segments between *electrodes 1 and 2* and between *electrodes 2 and 3*, respectively. *C*: the logarithm (ln) of mean sEPSP amplitude attenuation shown as a function of distance between 2 recording electrodes ($n = 10$ cells). A logarithmic attenuation factor of unity represents sEPSP peak voltage attenuation to $1/e$. Attenuations of different distances for the same propagation direction add linearly and can be fitted with a straight line through the origin. The corresponding distance to a value of 1 of ln attenuation (arrows; reflecting the AC correlate of the DC current length constant) gives the distance over which a sEPSP attenuates to $1/e$. This is 273 μm for somatopetal sEPSPs and 446 μm for somatofugal sEPSPs, respectively.

constant for typical EPSPs. This approximation seems justified since the attenuation of EPSPs is independent of rise time for rise times longer than 1–2 ms (Larkum et al. 1998).

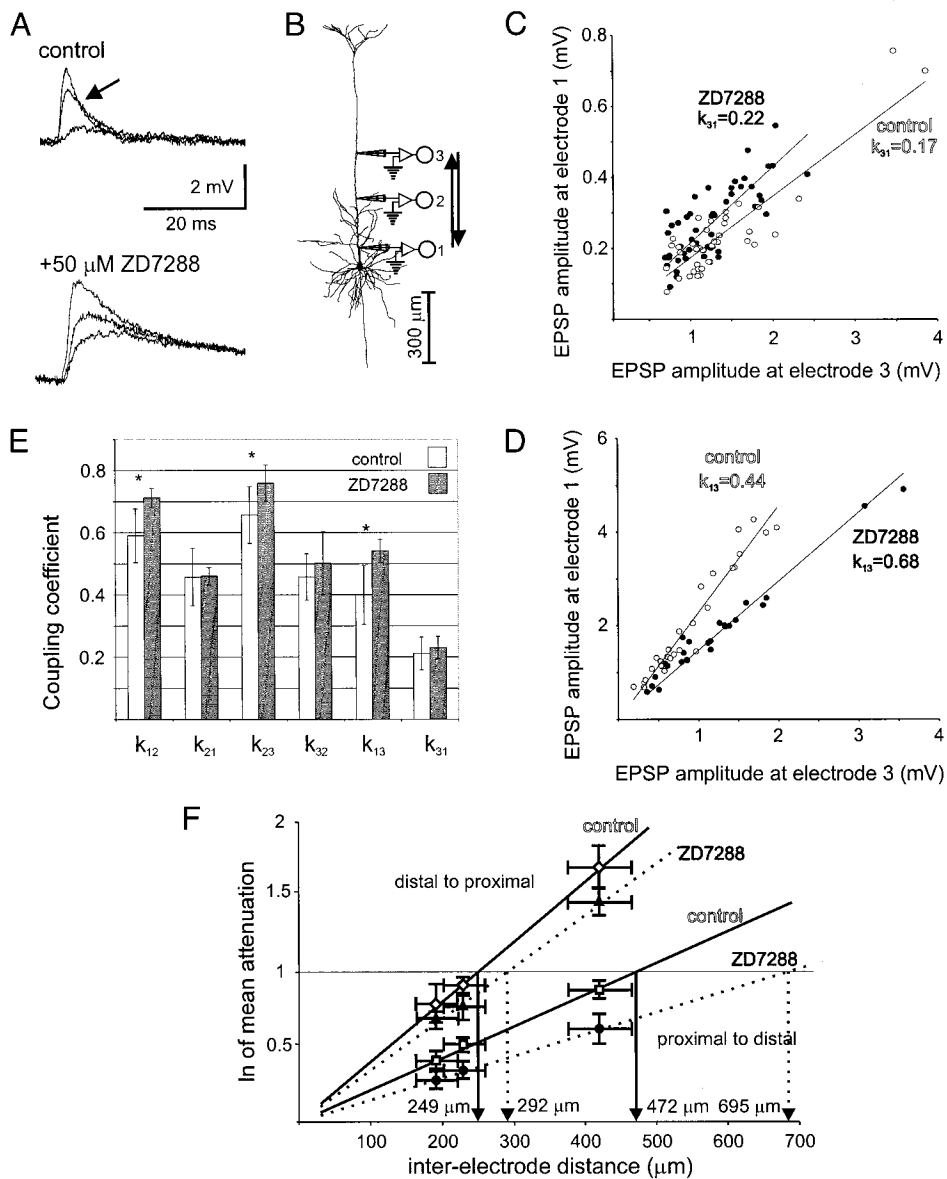


FIG. 4. Change in EPSP shape, coupling coefficients, and “AC length constants” after application of ZD7288. *A*: spontaneous EPSPs are recorded under control conditions (*top*) and with 50 μM ZD7288 (*bottom*) from the cell shown in *B*. They are superimposed and the presumed site of origin can be judged from their amplitude attenuation. Both are presumably generated distal to electrode 3 (comparable to Fig. 2*B*). Notice the crossing over of the falling phases of the EPSPs (\leftarrow) under control conditions, which disappears under ZD7288. In addition, a substantial increase in EPSP amplitude and area can be seen compared with the control EPSPs. *C* and *D*: coupling coefficients determined as described in Fig. 3*A* for spontaneous EPSPs traveling from distal to proximal (*C*) and from proximal to distal (*D*) under control conditions (\circ) and with ZD7288 (\bullet). *E*: comparison of the different coupling coefficients under control conditions (light gray bars; $n = 10$ cells) and with ZD7288 (dark gray bars; $n = 6$ cells). *F*: the logarithm (\ln) of mean EPSP amplitude attenuation ($\pm\text{SD}$) is plotted against the mean distance between the electrodes ($\pm\text{SD}$) for the 6 coupling coefficients calculated. Direct comparison of peak voltage attenuation of spontaneous EPSPs for 5 experiments under control conditions (\circ) and with ZD7288 (\bullet). While the EPSPs attenuates to $1/e$ at a distance of 249 μm under control, this value increases to 292 μm under ZD7288 for somatopetal EPSPs. The corresponding values increase from 472 to 695 μm for EPSPs traveling from soma to dendrite (reflecting the AC correlate of the DC current length constant).

Effects of I_h block on coupling coefficients and “length constants”

Under control conditions, sEPSPs spreading from dendrite to soma show an undershoot and a crossing over in the falling phase (Fig. 4*A*). After the application of ZD7288, undershoot and crossing over always disappear (Fig. 4*A*, *bottom*). The coupling coefficients increased significantly ($P < 0.05$) for somatofugal sEPSPs only while there was no significant increase in the opposite direction ($n = 5$ experiments; Fig. 4, *C–E*). This suggests that the I_h conductance must be situated on the distal part of the apical dendrite, generating a current load at the tuft.

Block of the I_h leads to an increase in the “AC length constant” of the dendrite. The mean inter-electrode distance was plotted against the average \ln of mean attenuation for all three dendritic segments under control and with I_h block ($n = 5$ experiments; Fig. 4*F*). Regression lines through each set of data points were used to estimate the distance over which

typical sEPSPs attenuate to $1/e$ in both directions. The nearly perfect correlation suggests that attenuation of sEPSPs is similar in the proximal and distal segment as well as over the combined section of both segments despite the fact that the distal segments tend to be slightly smaller in diameter than the proximal segments. The mean “length constant” of somatopetal sEPSPs increased by 17% from 249 to 292 μm under I_h block. However, this parameter increased more strongly for somatofugal sEPSPs with ZD7288 (from 472 to 695 μm , or 47% more).

The observation, that the coupling coefficient is not decreasing with increasing sEPSP amplitude (≤ 4 mV measured at the proximal electrode) suggests the absence of a voltage-dependent “boosting” (Figs. 3 and 4). sEPSPs are in fact strongly attenuated by the presence of an I_h conductance somewhere in the apical dendrite. Hence this additional attenuation is more pronounced for sEPSPs spreading in the somatofugal than in the somatopetal direction.

Summation properties of the apical dendrite

Neocortical cells *in vivo* often discharge in short bursts of high frequency (Helmchen et al. 1999; Zhu and Connors 1999), eliciting a brief train of EPSPs in the postsynaptic cell. We have simulated this situation by injecting five double-exponential waveforms at 50-Hz frequency (peak amplitude = 500 pA; $\tau_{\text{on}} = 0.4$ ms; $\tau_{\text{off}} = 5$ ms) (cf. Magee 1999a). The reciprocity test for such a waveform resulted in a perfect superposition of the two voltage transients recorded at each reciprocal electrode pair, suggesting linear behavior of the investigated neuron (Fig. 5A). This was true for control conditions and in the presence of ZD7288. The temporal summation properties of the cells were studied by injecting the current waveform into one electrode and recording the resulting voltage transients in the other two electrodes (Fig. 5B).

The peak amplitudes of the first compared with the fifth EPSP under control condition showed nearly no temporal summation, independent of location and length of the dendritic segments over which the burst of EPSPs spread ($n = 4$ cells; Fig. 5, C–E). Summation increased under blocking

conditions (Fig. 5, C–E). This increase was proportional to the length of the dendritic segment over which the EPSPs traveled but independent of the direction of EPSP propagation (Fig. 5, D and E). This symmetry in the summation behavior under control conditions and with ZD7288 was expected because the reciprocity test led to perfect superposition of reciprocal voltage transients.

With these experiments, it was clearly shown that an I_h conductance has a high impact on EPSP spread along the apical dendrite of layer V pyramidal cells. To study in detail its biophysical properties and the localization on the somatodendritic compartment of this cell type, voltage-clamp recordings were made.

Somatic whole cell voltage-clamp recordings of I_h

When pyramidal cells were hyperpolarized from a holding potential (V_{hold}) of -50 mV to potentials between -60 and -130 mV, all showed an inward current (termed hyperpolarization-activated current, I_h ; $n = 110$; Fig. 6A, control) as expected from the presence of a sag in all cells studied under

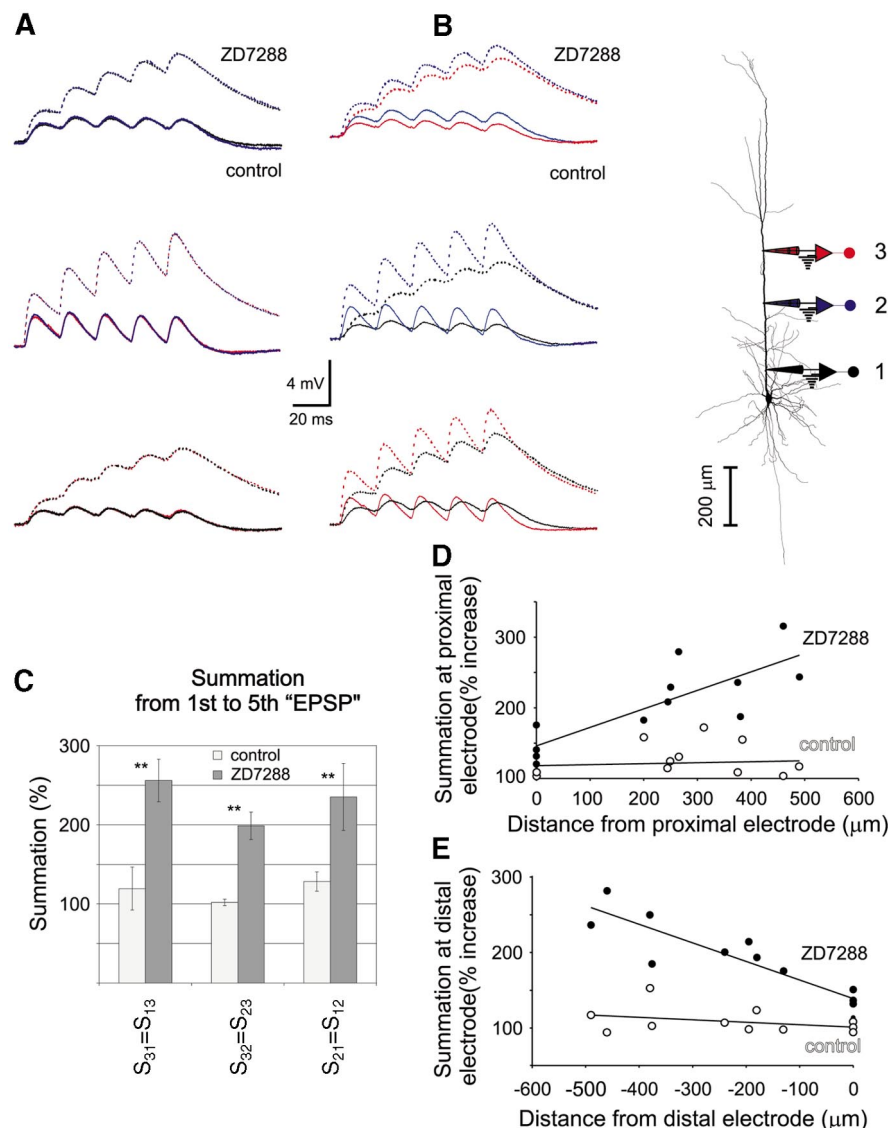


FIG. 5. Temporal summation properties of EPSP bursts. **A** and **B**: 5 double-exponential current waveforms (peak amplitude = 500 pA; $\tau_{\text{on}} = 0.4$ ms; $\tau_{\text{off}} = 5$ ms, 50-Hz frequency) were injected into the dendrite shown in Fig. 1, and the induced EPSP-like voltage responses were recorded. **A**: reciprocity test of the summation properties under control conditions (—) and with 50 μM ZD7288 (- - -). The current pulses were injected consecutively in each of a pair of electrodes and the resulting voltage response at the other electrode is displayed. For better comparison, these reciprocally obtained traces are superimposed. The color of the traces corresponds to the color code of the recording electrodes indicated in the diagram. Each reciprocal pair superimposes perfectly, again indicating linear properties. The application of ZD7288 leads to a marked increase in the amplitude of the later "EPSPs" due to temporal summation. **B**: summation properties were studied with the same waveform under control conditions (—) and with ZD7288 (- - -). Current was injected into 1 electrode, and the simultaneously recorded voltage transients from the 2 other electrodes are displayed. As in **A**, the color of the traces corresponds to the color code of the recording electrodes. **C**: temporal summation is expressed as the percentage change in amplitude between the peak of the 5th and the 1st "EPSP." This is shown for both control conditions and after application of ZD7288 for the 3 combinations of current injection and recording sites ($n = 4$ cells). **D**: EPSP summation at the proximal electrode plotted against the distance of current injection site under control conditions (\circ) and in the presence of ZD7288 (\bullet). Note that summation recorded at the proximal electrode increases with increasing distance of the current injection site, if I_h is blocked. With I_h present, little or no temporal summation is seen. **E**: EPSP summation recorded at the distal electrode plotted against the distance of current injection under control conditions (\circ) and with ZD7288 (\bullet). Note that without I_h , summation increases at the distal recording site with increasing distance of the current injection site, whereas with I_h , little or no temporal summation is seen.

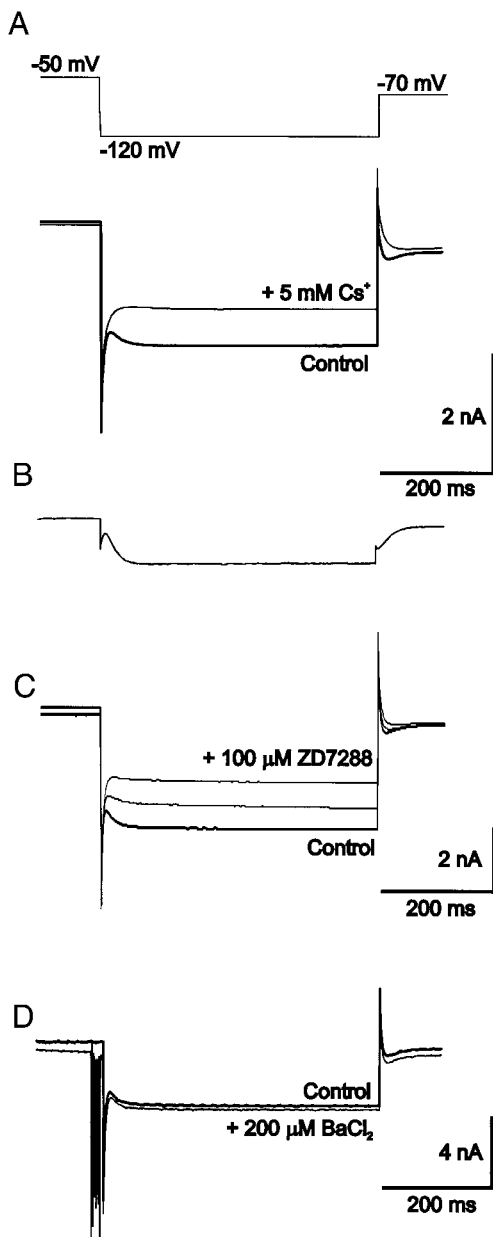


FIG. 6. I_h current is blocked by extracellular Cs^+ and intracellular ZD7288 but unaffected by barium. *A*: a P28 pyramidal cell was hyperpolarized in whole cell mode as indicated. A slowly rising inward current was activated and did not inactivate (control). After the end of the command pulse, a tail current could be seen. Application of 5 mM Cs^+ in the bath solution blocked the inward current as well as the tail current (thin line). Under these conditions, the cell became hyperpolarized. *B*: subtraction of the current in the presence of Cs^+ from the control current revealed the Cs^+ -sensitive component. *C*: a recording at the soma of a layer V pyramidal neuron (P30) with a pipette solution containing 100 μM ZD7288. Currents directly after establishing the whole cell mode (thick line), as well as 18 and 29 min later are superimposed (thin lines; from bottom to top). *D*: bath application of 200 μM BaCl_2 did not affect the I_h current (P31 rat). After the addition of barium, the cell depolarized and spontaneous bursts were generated (thin line).

current-clamp conditions (Fig. 1, *A* and *C*). The amplitude of the tail currents after clamping the cell from the hyperpolarizing pulse commands back to a V_h of -70 mV still increased even after a pulse to -160 mV indicating an insufficient space clamp. Therefore no further whole cell recordings were used to study the biophysical properties of I_h .

Block of I_h

Bath application of 5 mM CsCl (Fig. 6, *A* and *B*; $n = 15$) or 100 μM ZD7288 ($n = 3$) blocked I_h whole cell currents completely (see also Fain et al. 1978; Harris and Constanti 1995). In addition, the resting membrane potential hyperpolarized by ~ 10 – 15 mV. This suggested a reversal potential of the blocked conductance more depolarized than the resting potential. In contrast, bath application of 1 μM TTX, 200 μM 4-aminopyridine, or 10 mM TEA-Cl did not alter the I_h current at all ($n = 22$, not shown). It has been shown that ZD7288 exerts its blocking effect at the intracellular side of I_h channels (Harris and Constanti 1995), and therefore we have also used 100 μM ZD7288 in the pipette solution. It took 12–29 min until the I_h was completely blocked ($n = 3$), pointing to a localization of the I_h channels remote from the somatic drug injection (Fig. 6*C*). A blocking effect was also found by intracellular application of 10 mM QX 314 ($n = 3$; not shown), a substance primarily used to block voltage-gated sodium channels but that has been shown to block I_h (Perkins and Wong 1995). To prevent a possible confusion with inwardly rectifying potassium conductances (K_{ir}) (Takigawa and Alzheimer 1999), 200 μM BaCl_2 was applied to the bath. This resulted in a depolarization of the resting membrane potential, leading to fast trains of inward currents underlying spontaneous burst firing. I_h was not affected at all by BaCl_2 (Fig. 6*D*). These pharmacological tools identified the hyperpolarization-activated current found in neocortical layer V pyramidal cells unequivocally as I_h .

Dendritic localization of I_h

After the whole cell recording of I_h currents, a nucleated patch was excised from nine cells (Sather et al. 1992) (diameter ~ 10 μm ; i.e., the nucleated patch contained $\sim 20\%$ of the total somatic surface). No I_h current could be detected in any nucleated patch, although it was clearly present in the previous whole cell measurements (Fig. 7, *A* and *B*). In contrast, large voltage-gated K^+ and small Na^+ currents could be seen following depolarization of the nucleated patches (Fig. 7*C*) (for comparison, see Bekkers 2000; Korngreen and Sakmann 2000). Thus the lack of I_h currents in the nucleated patches could not be due to an artifact of the recording. When patching the dendrite of the cell from which the nucleated patch was excised (≤ 50 – 100 μm from the soma), I_h currents were detected again ($n = 3$; Fig. 7*D*).

These data suggest that I_h is not present or in extremely low densities at the soma of the layer V pyramidal cells. To better characterize the distribution of I_h along the cell, we made cell-attached patches on basal dendrites, the soma, and the apical dendrite up to a distance of 820 μm from the soma using a high- K^+ pipette solution. At the end of the cell-attached recording, the patch was ruptured to measure the resting membrane potential. The sum of this value and the voltage commands applied revealed the approximate holding potentials.

I_h currents were activated in cell-attached recordings at the apical dendrite at different distances from the soma and the biocytin-filled cell was reconstructed afterward. I_h current density was low up to a distance of ~ 400 μm from the soma and

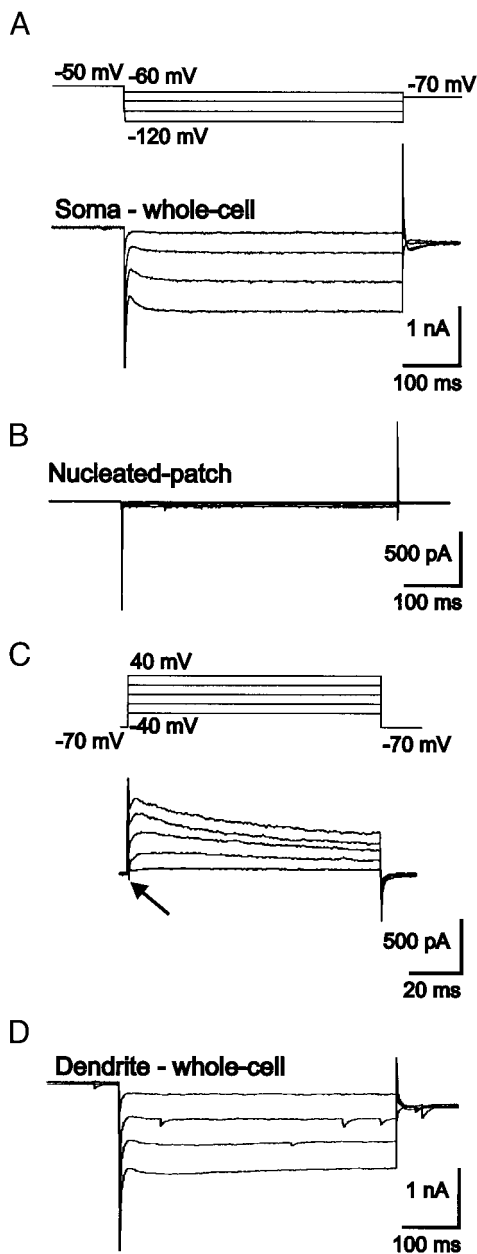


FIG. 7. I_h is not situated on the soma. *A*: I_h currents were induced with hyperpolarizing voltage commands as indicated using a patch pipette at the soma of a layer V pyramidal neuron (P28). *B*: the same protocol did not elicit a similar current in the nucleated patch of the same cell. *C*: in contrast, depolarizing pulses induced small Na^+ (\leftarrow) as well as K^+ currents in the nucleated patch. *D*: patch recordings from the apical dendrite of the same cell again revealed I_h currents using the same protocol as in *A*.

increased markedly more distally (Fig. 8A). When the current densities measured in 60 patches from 35 cells were plotted as a function of the distance of the recording site from the soma (Fig. 8B), a consistent pattern of current density was found across all neurons. While we found only a low mean I_h density of $\sim 3 \text{ pA}/\mu\text{m}^2$ in the soma, basal dendrites, and apical dendrites up to $\sim 400 \mu\text{m}$, there was a nonlinear 13-fold increase in the more distal dendrites. The maximal I_h density was in the range of $40 \text{ pA}/\mu\text{m}^2$ reflecting a conductance of $\sim 0.03 \text{ S}/\text{cm}^2$ (Fig. 8B).

Biophysical properties of I_h

I_h currents were activated by clamping cell-attached patches for 500 ms from approximately -45 mV to values between -85 and -155 mV . The activation became faster at more hyperpolarized V_{hold} (Fig. 9, A and C), and time constants τ were evaluated for the current rise during the 100 ms after the onset of the pulse (see - - - in Fig. 9A). They were in the range between $31 \pm 9 \text{ ms}$ at -85 mV and $13 \pm 1 \text{ ms}$ at -155 mV

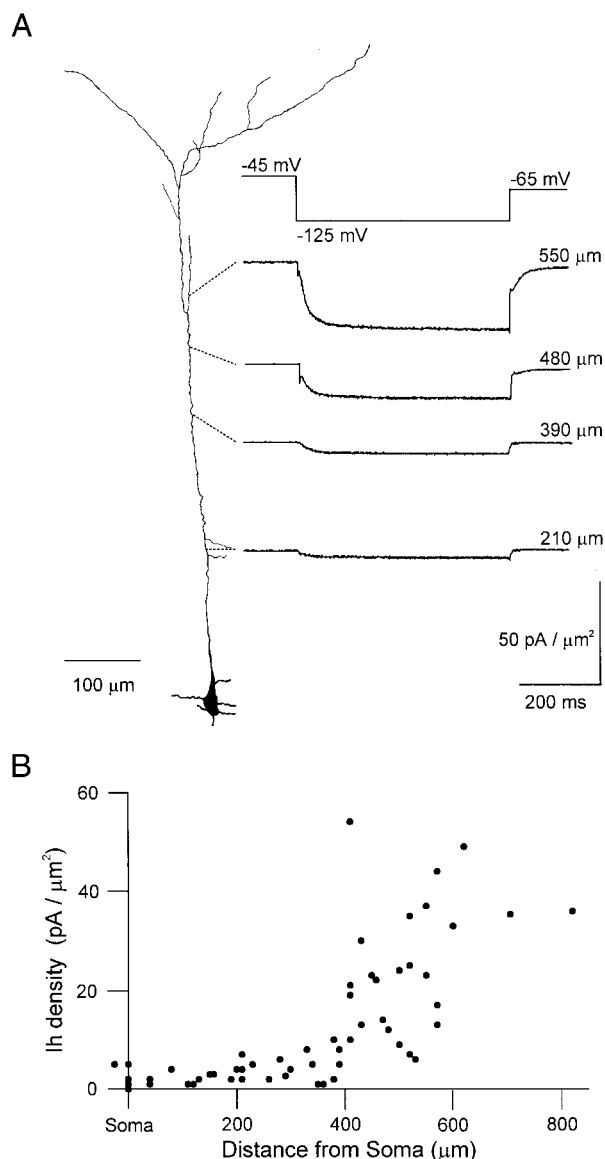


FIG. 8. I_h is situated on the distal apical dendrite. *A*: consecutive cell-attached patches along the apical dendrite of a layer V pyramidal neuron (P29) at different patches from the soma using a high- K^+ pipette solution. Hyperpolarizing voltage commands to approximately -125 mV resulted in the activation of tiny I_h currents at distances smaller than $400 \mu\text{m}$ from the soma, while at more distal recording sites a large I_h current flow could be induced. After the cell-attached recordings, the cell was filled with biocytin by going to whole cell mode. *B*: the I_h current densities from 60 cell-attached recordings were plotted against their distance from the soma. While on the basal dendrites, the soma, and the apical dendrite $\leq 400 \mu\text{m}$ nearly no I_h currents could be found, more distal recordings $\leq 820 \mu\text{m}$ showed a marked nonlinear increase in I_h density.

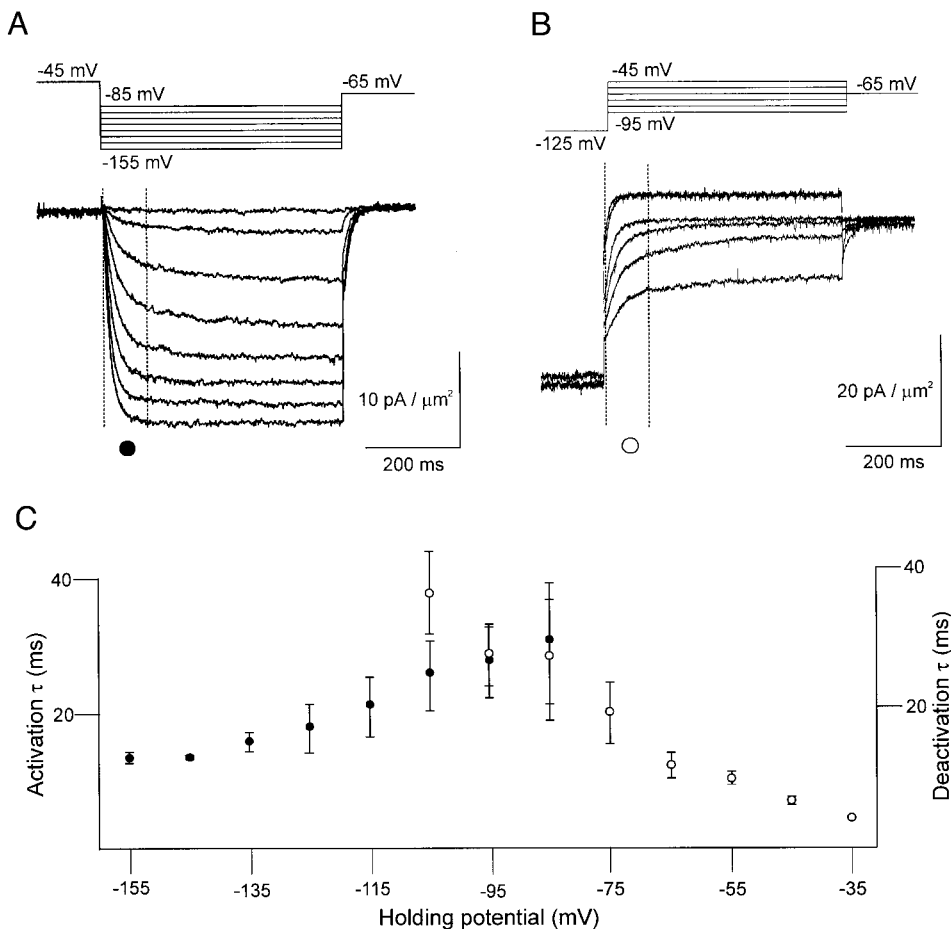


FIG. 9. Activation and deactivation kinetics of the I_h . *A*: in the cell-attached patch of the cell shown in Fig. 8*A* (distance from soma $550 \mu\text{m}$), I_h currents were activated with hyperpolarizing clamp commands as indicated. The rising phase of the current was fitted between --- with a monoexponential function. *B*: in the same patch, I_h currents were fully activated with a hyperpolarizing pulse and then deactivated with depolarizing commands as indicated. As in *A*, the falling phase of the current was fitted between --- with a monoexponential function. *C*: using the fits from 5 cells, the mean activation (\bullet) and deactivation (\circ) time constants were plotted against the holding potential applied.

($n = 5$; Fig. 9*C*). If I_h was activated with a 500-ms pulse to approximately -125 mV and thereafter deactivated at different V_{hold} between -105 and -35 mV , the deactivation became faster with more depolarized V_{hold} (Fig. 9*B*). Time constants were evaluated for the current decay during a 100-ms interval after the end of the pulse (see --- in Fig. 9*B*). They were in the range of $37 \pm 6 \text{ ms}$ at -105 mV and $7 \pm 1 \text{ ms}$ at -45 mV ($n = 4$; Fig. 9*C*).

After the end of an activating pulse, a tail current could be detected (Fig. 10*A*). The amplitude of this current measured directly after the end of the pulse (see --- in Fig. 10*A*) was plotted against the V_{hold} of the previous pulse command. These relations from five cells were normalized and fitted with a Boltzmann function (Fig. 10*B*). The value for half-maximal activation and steepness of the Boltzmann fit were evaluated for each cell ($n = 5$) and averaged. A half-maximal activation at $-94.8 \pm 6.4 \text{ mV}$ and an e -fold current response per $7.8 \pm 1.7 \text{ mV}$ voltage change were found.

The reversal potential (E_h) of I_h was estimated from the deactivation protocol shown in Fig. 9*B*. I_h currents in cell-attached recordings had a reversal at $4.5 \pm 6.8 \text{ mV}$ using a high- K^+ pipette solution ($n = 4$; not shown). With a high- Na^+ pipette solution or in whole cell mode, this parameter shifted to its physiological value of $-47.7 \pm 3.8 \text{ mV}$ ($n = 4$; not shown). Using the GHK equation a permeability ratio for $\text{P}_{\text{Na}^+}^+/\text{P}_{\text{K}^+}^+$ of ~ 0.4 was calculated.

DISCUSSION

The following main findings were obtained. 1) The perfect reciprocity between spatially separated locations indicates that layer V cells can be treated as a linear system at resting potential and for voltage deflections in the range of spontaneous synaptic events. 2) Attenuation of sEPSPs along this apical dendrite is considerably larger than expected for a passive cable with standard values of membrane resistivity and uniform conductance distribution, particularly for somatofugal sEPSPs. This is due to the presence of a hyperpolarization-activated current (I_h). 3) Furthermore this conductance tends to prevent the summation of EPSP-like events irrespective of the location of current injection along the apical dendrite. And 4) the I_h conductance is located preferentially on the distal apical dendrite in a very high density and has relatively fast kinetics.

Layer V pyramidal cell is a linear system in the voltage range of EPSPs

In a linear system, consecutive and reciprocal current injection in a pair of electrodes leads to an identical voltage response in the second electrode (reciprocity rule). This is true for layer V pyramidal neurons at resting membrane potential $\pm 4 \text{ mV}$. This does not, however, imply that the attenuation is the same in both directions since the same current injection results in different voltage responses at the different injection sites. For the voltage deflections studied,

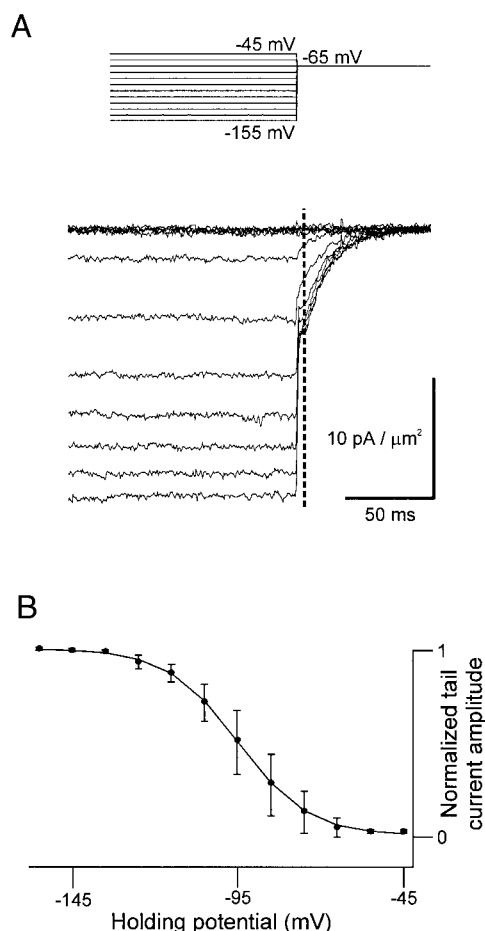


FIG. 10. Activation range of I_h . *A*: in the same cell-attached patch shown in Fig. 9A, I_h currents were activated with hyperpolarizing clamp commands as indicated. After their offset, tail currents could be seen at the resting potential. *B*: the amplitude of these tail currents was obtained at the position marked by --- in *A* and normalized for 5 cells. The mean tail current amplitude was plotted against the holding potential applied before. A Boltzmann function was used to fit this activation function. The steepness of the Boltzmann function is underestimated due to the averaging procedure.

the nonlinearity introduced by I_h is not seen in the reciprocity test. This is due to the remote localization of the I_h in the distal dendrite and its hyperpolarized activation range. Therefore the current spread in the proximal dendrite appears to be linear.

By comparing sEPSP propagation at three sites along the apical dendrite, we were able to examine the homogeneity of dendritic membrane properties for subthreshold events. The coupling coefficients were similar for both the proximal and distal segments (Fig. 3B), suggesting that the first half of the apical dendrite (up to $\sim 500 \mu\text{m}$) has homogeneous passive membrane properties. However, blocking I_h with ZD7288 resulted in a stronger hyperpolarization of resting potential at more distal electrodes [this depolarizing impact of the I_h has also been described in other cell types (e.g., Holt and Eatock 1995)]. Thus beyond the distal electrode, an increasing I_h density must be expected. In addition, cable properties predict that boundary effects should play an ever increasing role as signals approach the distal dendritic tips.

Attenuation for voltage signals spreading along the dendrite is larger than expected for a passive cable with homogeneous

conductance distribution (see also Schwandt and Crill 1997; Stuart and Spruston 1998). This attenuation represents a measure of the influence that subthreshold signals have on the axonal site of integration as a function of distance from the soma. Attenuation is stronger for somatopetal sEPSPs reflected by a smaller "AC length constant." This difference is due to the large electrical load that the soma together with the basal dendrites represents for the approaching EPSP. This difference was predicted for motoneurons (Rall 1962) and was recently experimentally verified in cultured motoneurons (Larkum et al. 1998). In contrast, EPSPs at electrotonically remote sites may overcome this attenuation if they are large enough to activate additional calcium conductances (Cauller and Connors 1994; Larkum et al. 1999b; Yuste et al. 1994). Our results suggest that "boosting" does not occur for small voltage deflections like EPSPs along the apical dendrite (amplitude ≤ 4 mV at the proximal electrode). EPSP amplification has been reported for large voltage deflections or under depolarized conditions due to the activation of a persistent sodium current for depolarizations of ≥ 15 mV at the soma (Schwandt and Crill 1995; Stuart and Sakmann 1995; Williams and Stuart 2000). We did not measure attenuation in either of these cases.

Summation of EPSPs is prevented by the presence of an I_h conductance

Summation was determined by comparison of the amplitudes of the first and the fifth EPSP of a train (Fig. 5). We observed that the summation of a train of EPSP-like waveforms at 50 Hz under control conditions was negligible and independent on location and distance of injection and recording electrode. This is true also in CA1 pyramidal neurons (Cash and Yuste 1998; Magee 1999a). Application of the I_h blocker ZD7288 led to location-dependent summation (see also Williams and Stuart 2000). If the EPSP train is injected far away from the recording electrode, summation becomes larger due to the temporal dispersion of the single EPSP waveform. This is true for both propagation directions (Fig. 5, *D* and *E*). The I_h masks therefore the passive summation properties of the cell by curtailing the EPSP and generating an undershoot in its decay time course (see also Williams and Stuart 2000).

Nonuniform distribution of I_h

The attenuation of sEPSPs was markedly reduced when the I_h conductance was blocked. In addition, this block led to the disappearance of the undershoot and crossing over of distally originating sEPSPs. Crossing over has been shown in pyramidal neurons for somatopetal events and models with nonuniform conductance distributions are expected to give crossing over (Koch 1999; London et al. 1999; Magee 1999a; Nicoll et al. 1993; Stuart and Spruston 1998; Williams and Stuart 2000). Cell-attached recordings from different compartments of the neocortical pyramidal cell revealed a high density of the I_h in the apical dendrite more distant than $400 \mu\text{m}$ from the soma ($\leq 40 \text{ pA}/\mu\text{m}^2$ or $0.03 \text{ S}/\text{cm}^2$). This nonlinear increase resulted in an extremely uneven I_h distribution, even more pronounced than found in CA1 pyramidal cells (Magee 1998). In another study of layer V pyramidal cells, Williams and Stuart (2000) have described the I_h channel density up to $\sim 400 \mu\text{m}$ from the soma. They missed the dramatic increase beyond this point that

was revealed in this study because we extended our recordings $\leq 820 \mu\text{m}$ from the soma. The soma itself, the basal dendrites and the proximal apical dendrite were practically devoid of the I_h conductance. A similar distribution was also found in an immunohistochemical study of HCN-1 (Santoro et al. 1997), one of the four cloned I_h subunits.

Kinetics and modulation of the I_h

The kinetics of activation and deactivation of the I_h in our study can be well described by a monoexponential function with a τ of ~ 30 ms at half-maximal activation. The kinetic data found in this study are nearly identical to those found by Williams and Stuart (2000) in another study on I_h currents in cell-attached recordings from layer V pyramidal cells. In addition, some cells showed the presence of a second slow exponential function of lower weight. There is a large variability in the published data for the I_h kinetics in different native cell types (see Santoro and Tibbs 1999). Nevertheless all data can be roughly classified according to the speed of activation. One group of I_h channels with time constants in the range of hundreds of milliseconds is present in heart and thalamus, presumably reflecting the presence of the slowly gating HCN-2 or HCN-4 subunits of the I_h channels (Seifert et al. 1999). In contrast, the time constants of the other group are much faster ($\tau < 100$ ms). They are found in various central neurons outside the thalamus and may reflect the presence of fast HCN-1 subunits (Ludwig et al. 1998; Santoro et al. 1998, 2000). In pyramidal cells of layer V as well as of the CA1 hippocampus, the presence of the HCN-1 subunit has been shown by in situ hybridization (Mossmang et al. 1999; Santoro et al. 2000), immunocytochemistry (Santoro et al. 1997), and single-cell PCR (Franz et al. 2000). In addition, the half-maximal activation at -95 mV is comparable to the data from HCN-1 transcripts. Thus the subunits underlying the I_h conductance studied here are likely to be coded by the HCN-1 gene.

It is well known that I_h in heart and thalamus can be modulated by various G-protein-coupled events (Di Francesco and Tortora 1991; Lüthi and McCormick 1998). This ability seems to be due to the underlying HCN-4 subunits which are highly cyclic nucleotide sensitive while HCN-1 subunits are not (see Santoro and Tibbs 1999). Therefore we would not expect a large effect of cyclic nucleotides on the I_h in layer V pyramidal cells due to its molecular constituents.

Functional implications

One effect of a distal region with a high density of I_h is to isolate the two spike initiation zones from each other with respect to the inputs integrated. Back-propagating action potentials are larger than expected for passive dendrites due to the active boosting by Na^+ channels. On the other hand, due to I_h , EPSPs transmitted in both directions are smaller than expected from a passive uniform cable model. This effect is especially marked for high-frequency synaptic input. Thus subthreshold events have a disproportionately low influence on the remote spike initiation zone, whereas suprathreshold events have a disproportionately high influence. The high I_h density in the distal apical dendrite introduces a large electric load comparable to that of the soma resulting in an increase of the electro-

tonic distance between the two spike initiation zones. This may therefore be an effective means of confining the integration of synaptic inputs to one or the other of the two spike initiation zones while only the crossing of threshold is effectively transmitted to the other initiation zone. In addition, a distal region with a high density of I_h could also prevent large EPSPs from approaching their reversal potential. A reduced EPSP saturation would lead to linearization of the relationship between presynaptic input frequency and postsynaptic response (Bernander et al. 1994) and therefore a larger dynamic range.

We thank K. de Peyer for excellent technical assistance and Drs. J. Bischofberger, H.-P. Clamann, W. Senn, and D. Ulrich for helpful discussions and for carefully reading this manuscript.

This work was supported by the Swiss National Science Foundation (Grant SNF 3100-042055.94 to H.-R. Lüscher) and the Silva Casa Stiftung.

REFERENCES

- BERNANDER Ö, KOCH C, AND DOUGLAS RJ. Amplification and linearization of distal synaptic input to cortical pyramidal cells. *J Neurophysiol* 72: 2743–2753, 1994.
- BEKKERS J. Properties of voltage-gated potassium currents in nucleated patches from large layer 5 cortical pyramidal cells of the rat. *J Physiol (Lond)* 525: 593–609, 2000.
- CARNEVALE NT AND JOHNSTON D. Electrophysiological characterization of remote chemical synapses. *J Neurophysiol* 47: 606–621, 1982.
- CASH S AND YUSTE R. Input summation by cultured pyramidal neurons is linear and position-independent. *J Neurosci* 18: 10–15, 1998.
- CAULLER LJ AND CONNORS BW. Synaptic physiology of horizontal afferents to layer I in slices of rat SI neocortex. *J Neurosci* 14: 751–762, 1994.
- DI FRANCESCO D AND TORTORA P. Direct activation of cardiac pacemaker channels by intracellular cyclic AMP. *Nature* 351: 145–147, 1991.
- FAIN GL, QUANDT FN, AND BASTIAN BL. Contribution of a cesium-sensitive conductance increase to the rod photoresponse. *Nature* 272: 467–469, 1978.
- FRANZ O, LISS B, NEU A, AND ROEPER J. Single-cell mRNA expression of HCN1 correlates with a fast gating phenotype of hyperpolarization-activated cyclic nucleotide-gated ion channels (Ih) in central neurons. *Eur J Neurosci* 12: 2685–2693, 2000.
- HARRIS NC AND CONSTANTIN A. Mechanism of block by ZD 7288 of the hyperpolarization-activated inward rectifying current in guinea pig substantia nigra neurons in vitro. *J Neurophysiol* 74: 2366–2378, 1995.
- HELMCHEN F, SVOBODA K, DENK W, AND TANK DW. In vivo dendritic calcium dynamics in deep-layer cortical pyramidal neurons. *Nat Neurosci* 2: 989–996, 1999.
- HOLT JR AND EATOCK RA. Inwardly rectifying currents of saccular hair cells from the leopard frog. *J Neurophysiol* 73: 1484–1502, 1995.
- HSU SM, RAINE L, AND FANGER H. The use of avidin-biotin-peroxidase complex (ABC) in immunoperoxidase techniques: a comparison between ABC and unlabelled antibody (peroxidase) procedures. *J Histochem Cytochem* 29: 577–590, 1981.
- JOHNSTON D, MAGEE JC, COLBERT CM, AND CHRISTIE BR. Active properties of neuronal dendrites. *Annu Rev Neurosci* 19: 165–186, 1996.
- KOCH C. *Biophysics of Computation*. New York: Oxford, 1999.
- KORNGREEN A AND SAKMANN B. Voltage-gated K^+ channels in layer 5 neocortical pyramidal neurones from young rats: subtypes and gradients. *J Physiol (Lond)* 525: 621–639, 2000.
- LARKUM ME, KAISER KMM, AND SAKMANN B. Calcium electrogenesis in distal apical dendrites of layer 5 pyramidal cells at a critical frequency of back-propagating action potentials. *Proc Natl Acad Sci USA* 96: 14600–14604, 1999a.
- LARKUM ME, LAUNY T, DITYATEV A, AND LÜSCHER H-R. Integration of excitatory postsynaptic potentials in dendrites of motoneurons of rat spinal cord slices cultures. *J Neurophysiol* 80: 924–935, 1998.
- LARKUM ME, RIOULT MG, AND LÜSCHER H-R. Propagation of action potentials in the dendrites of neurons from rat spinal cord slice cultures. *J Neurophysiol* 75: 154–169, 1996.
- LARKUM ME, ZHU JJ, AND SAKMANN B. A new cellular mechanism for coupling inputs arriving at different cortical layers. *Nature* 398: 338–341, 1999b.

- LONDON M, MEUNIER C, AND SEGEV I. Signal transfer in passive dendrites with nonuniform membrane conductance. *J Neurosci* 19: 8219–8233, 1999.
- LUDWIG A, ZONG X, JEGELITSCH M, HOFMANN F, AND BIEL M. A family of hyperpolarization-activated mammalian cation channels. *Nature* 393: 587–591, 1998.
- LÜTHI A AND McCORMICK DA. Periodicity of thalamic synchronized oscillations: the role of Ca^{2+} -mediated upregulation of I_h . *Neuron* 20: 553–563, 1998.
- MAGEE JC. Dendritic hyperpolarization-activated currents modify the integrative properties of hippocampal CA1 pyramidal neurons. *J Neurosci* 18: 7613–7624, 1998.
- MAGEE JC. Dendritic I_h normalizes temporal summation in hippocampal CA1 neurons. *Nat Neurosci* 2: 508–514, 1999a.
- MAGEE JC. Voltage-gated ion channels in dendrites. In: *Dendrites*, edited by Stuart G, Spruston N, and Häusser M. New York: Oxford, 1999b, p. 139–160.
- MOOSMANG S, BIEL M, HOFMANN F, AND LUDWIG A. Differential distribution of four hyperpolarization-activated cation channels in mouse brain. *Biol Chem* 380: 975–980, 1999.
- NICOLL A, LARKMAN A, AND BLAKEMORE C. Modulation of EPSP shape and efficacy by intrinsic membrane conductances in rat neocortical pyramidal neurons in vitro. *J Physiol (Lond)* 468: 693–710, 1993.
- PAPE H-C. Queer current and pacemaker: the hyperpolarization-activated cation current in neurons. *Annu Rev Physiol* 58: 299–327, 1996.
- PERKINS KL AND WONG RKS. Intracellular QX-314 blocks the hyperpolarization-activated inward current I_q in hippocampal CA1 pyramidal cells. *J Neurophysiol* 73: 911–915, 1995.
- RALL W. Theory of physiological properties of dendrites. *Ann NY Acad Sci* 96: 1071–1092, 1962.
- RALL W. Distinguishing theoretical synaptic potentials computed for different soma-dendritic distributions of synaptic input. *J Neurophysiol* 30: 1138–1168, 1967.
- SANTORO B, CHEN S, LÜTHI A, PAVLIDIS P, SHUMYATSKY GP, TIBBS GR, AND SIEGELBAUM SA. Molecular and functional heterogeneity of hyperpolarization-activated pacemaker channels in the mouse CNS. *J Neurosci* 20: 5264–5275, 2000.
- SANTORO B, GRANT SGN, BARTSCH D, AND KANDEL ER. Interactive cloning with the SH3 domain of N-src identifies a new brain specific ion channel protein, with homology to Eag and cyclic nucleotide channels. *Proc Natl Acad Sci USA* 94: 14815–14820, 1997.
- SANTORO B, LIU DT, YAO H, BARTSCH D, KANDEL ER, SIEGELBAUM SA, AND TIBBS GR. Identification of a gene encoding a hyperpolarization-activated pacemaker channel of brain. *Cell* 93: 717–729, 1998.
- SANTORO B AND TIBBS GR. The HCN gene family: molecular basis of the hyperpolarization-activated pacemaker channels. *Ann NY Acad Sci* 868: 741–764, 1999.
- SATHER W, DIEUDONNÉ S, MACDONALD JF, AND ASCHER P. Activation and desensitization of *N*-methyl-D-aspartate receptors in nucleated outside-out patches from mouse neurones. *J Physiol (Lond)* 450: 643–672, 1992.
- SCHILLER J, SCHILLER Y, STUART G, AND SAKMANN B. Calcium action potentials restricted to distal apical dendrites of rat neocortical pyramidal neurons. *J Physiol (Lond)* 505: 605–616, 1997.
- SEIFERT R, SCHOLTEN A, GAUSS R, MINCHEVA A, LICHTER P, AND KAUPP UB. Molecular characterization of a slowly gating human hyperpolarization-activated channel predominantly expressed in thalamus, heart, and testis. *Proc Natl Acad Sci USA* 96: 9391–9396, 1999.
- SCHWINDT PC AND CRILL WE. Amplification of synaptic current by persistent sodium conductance in apical dendrite of neocortical neurons. *J Neurophysiol* 74: 2220–2224, 1995.
- SCHWINDT PC AND CRILL WE. Modification of current transmitted from apical dendrite to soma by blockade of voltage- and Ca^{2+} -dependent conductances in rat neocortical pyramidal neurons. *J Neurophysiol* 78: 187–198, 1997.
- STUART GJ, DODT H-U, AND SAKMANN B. Patch-clamp recordings from the soma and dendrites of neurons in brain slices using infrared video microscopy. *Pflügers Arch* 423: 511–518, 1993.
- STUART G AND SAKMANN B. Active propagation of somatic action potentials into neocortical pyramidal cell dendrites. *Nature* 367: 69–72, 1994.
- STUART G AND SAKMANN B. Amplification of EPSPs by axosomatic sodium channels in neocortical pyramidal neurons. *Neuron* 15: 1065–1076, 1995.
- STUART G AND SPRUSTON N. Determinants of voltage attenuation in neocortical pyramidal neuron dendrites. *J Neurosci* 18: 3501–3510, 1998.
- TAKIGAWA T AND ALZHEIMER C. G protein-activated inwardly rectifying K^+ (GIRK) currents in dendrites of rat neocortical pyramidal cells. *J Physiol (Lond)* 517: 385–390, 1999.
- WILLIAMS SR AND STUART GJ. Site independence of EPSP time course is mediated by dendritic I_h in neocortical pyramidal neurons. *J Neurophysiol* 83: 3177–3182, 2000.
- YUSTE R, GUTNICK MJ, SAAR D, DELANEY KR, AND TANK DW. Ca^{2+} accumulations in dendrites of neocortical pyramidal neurons: an apical band and evidence for two functional compartments. *Neuron* 13: 23–43, 1994.
- YUSTE R AND TANK DW. Dendritic integration in mammalian neurons, a century after Cajal. *Neuron* 16: 701–716, 1996.
- ZADOR AM, AGMON-SNIR H, AND SEGEV I. The morphoelectronic transform: a graphical approach to dendritic function. *J Neurosci* 15: 1669–1682, 1995.
- ZHU JJ AND CONNORS BW. Intrinsic firing patterns and whisker-evoked synaptic responses of neurons in rat barrel cortex. *J Neurophysiol* 81: 1171–1183, 1999.